# The COST 2100 Channel Model: Parameterization and Validation Based on Outdoor MIMO Measurements at 300 MHz

Zhu, Meifang; Eriksson, Gunnar; Tufvesson, Fredrik

*Published in:*
IEEE Transactions on Wireless Communications

*DOI:*
10.1109/TWC.2013.010413.120620

2013

# The COST 2100 Channel Model: Parameterization and Validation Based on Outdoor MIMO Measurements at 300 MHz

Meifang Zhu, *Student Member, IEEE,* Gunnar Eriksson, *Member, IEEE,*
and Fredrik Tufvesson, *Senior Member, IEEE*

***Abstract*—The COST 2100 channel model is a geometry-based stochastic channel model (GSCM) for multiple-input multiple-output (MIMO) simulations. This paper presents parameterization and validation of the channel model for peer-to-peer communication in the 300 MHz band. Measurements were carried out in outdoor environments for both line-of-sight (LOS) and non line-of-sight (NLOS) scenarios. The COST 2100 channel model is characterized and parameterized based on clusters. The KpowerMeans algorithm and a Kalman filter are used for identifying and tracking clusters from measurements. General issues regarding the parameterization of the channel model are analyzed in detail. A full set of single-link parameters for the channel model is extracted from the measurements. These parameters are used as the input to the channel model validation processes, targeting delay spread, spatial correlation, and singular value distribution as well as antenna correlation. The validation results show good agreement for the spatial correlation and singular value distribution between the channel model simulations and the 300 MHz outdoor measurements. Our findings suggest that the model has potential for modeling 300 MHz channels in outdoor environments, although some modifications are needed for the distribution of cluster delay spreads and the size of cluster visibility regions.**

***Index Terms*—Channel model, COST 2100, MIMO, outdoor, parameterization, validation.**

## I. Introduction

The channel model from COST 273 [1], and its successor COST 2100 [2] are now available and can account for most of the important propagation processes and effects that influence multiple-input multiple-output (MIMO) system performance. The COST 2100 channel model is characterized by individual clusters, i.e. groups of multipath components (MPCs) showing similar properties in delay, angle of arrival (AOA), angle of departure (AOD) and power, and corresponding visibility regions of the clusters [2]. The model supports both single-link and multiple-link MIMO channel access; the latter is achieved by using the concept of common clusters [3]. An overview of the COST 2100 channel model is presented in [4], whereas a detailed description of the channel model can be found in [2]. The parameterization of this generic model from measurements is not yet complete and only a few environments have been studied. For example, parameterization of the channel model has been performed for indoor environments though some parameters are missing, such as cross-correlation coefficients for cluster spreads, and cluster shadowing [5]. Furthermore, there is a lack of studies validating the COST 2100 channel model. One reason for this is that there is no general methodology to evaluate the validity of channel models, and the validation processes also depend on available measurement data and the nature and usage of the particular channel model. In [6], validation of the COST 2100 channel model, with respect to large-scale properties such as delay spread and angular spread, has been carried out for an indoor environment with good results. So far, studies on the COST 2100 channel model mostly focus on indoor environments, but are missing for outdoor scenarios. For a good generic model, different environments should be included and completely parameterized. In addition, validation should be performed to determine the accuracy and limitations of the channel model in those environments as well.

In order to perform parameterization and validation of the COST 2100 channel model in outdoor scenarios, 300 MHz outdoor measurements were performed and the collected data is used for further analysis in this paper. Frequencies in the lower UHF range, as used for the measurements, are often used for tactical communication. In addition, public cellular communication systems are present at 450 MHz and 900 MHz, and TETRA, a cellular and peer-to-peer system for first responders, operates at frequencies around 400 MHz. From a scientific point of view, it is also of interest to characterize propagation conditions at those frequencies as many common larger objects in the environments (like vehicles, smaller buildings, and lamp-posts) have the size of a few wavelengths instead of tens to hundreds of wavelengths as for the standard cellular frequencies. Hence, it is of significant interest to investigate and characterize the channel properties and provide a basis for the usage of the COST 2100 channel model at lower frequencies.

The main contributions of this paper are:

- Cluster parameters and cluster time-variant properties are obtained from the 300 MHz measurements by using a joint clustering and tracking algorithm.
- Parameterization of the channel model for single-link outdoor MIMO communication at 300 MHz is conducted.
- Validation of the channel model is performed for the considered scenario by comparing simulated and measured delay spreads, spatial correlations, singular value distributions and antenna correlations.

The remainder of the paper is organized as follows: Sec. II describes the 300 MHz outdoor measurement campaign. Sec. III introduces the joint clustering and tracking algorithm for

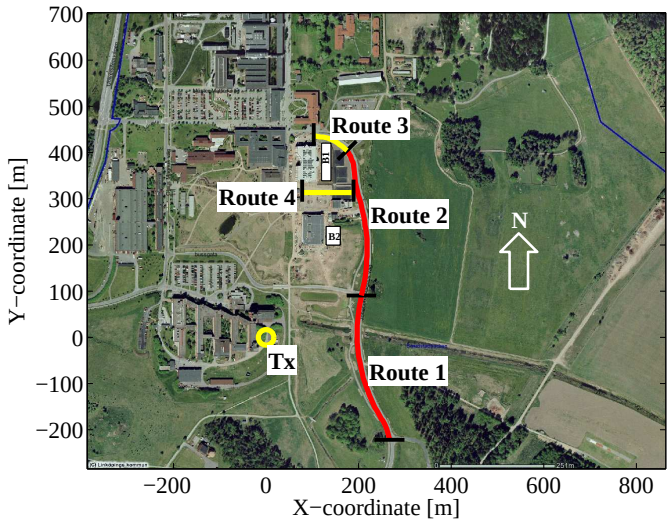


Fig. 1. Overview of the measurements area at the campus of Linköping University, Sweden. The transmitter with coordinate (0, 0) was placed near the building, and the receiver was moved along the marked routes 1-4. B1 and B2 represent two new buildings which were not present at the time the picture was taken.

cluster extraction from the measurements. The parameterization for the COST 2100 single-link MIMO channel model in an outdoor scenario is performed in Sec. IV. Sec. V validates the single-link parameters for the channel model. Finally, the conclusions in Sec. VI complete the paper.

## II. Measurement Campaign

The measurements were performed outdoors on the campus of Linköping University, Sweden using the RUSK Lund MIMO channel sounder [7], [8]; the measurement principle is described in [9], [10]. Identical antenna arrays were used for both the transmitter and the receiver. The antenna arrays are vertically polarized, 7-element uniform circular dipole arrays (UCDA), with one additional dipole element located at the center, in an elevated position [7], [11]. All 8 elements are sleeve dipoles and the center element, which has an omni-directional antenna response in azimuth, is located 0.78 m above the 7-element UCDA. The bandwidth of the antennas is 30 MHz, and the antenna gain for the UCDA is 8 dBi and 5 dBi for the omni-directional antenna. The 3 dB beam width of the lower antenna elements is 95 degrees in azimuth and 59 degrees in elevation. The transmit antenna array (Tx) was placed 1.8 m above ground, at a static position with coordinate (0, 0) and about 35 m from a large building. The receive antenna array (Rx) was mounted on a car with its lower ground plane approximately 2.1 m above the ground. The car was driven at a speed of around 8 m/s along the marked routes in Fig. 1, and the routes are labeled as 1 to 4. The minimum and maximum separation between the Tx and Rx are 197 m and 451 m, respectively. The measurements were carried out at a center frequency of 285 MHz, with a bandwidth of 20 MHz, which is smaller than the antenna bandwidth, and an output power of 43 dBm. The sounding signal is a periodically repeated sequence with a length of 12.8 μs and the guard interval between the repetitions is 12.8 μs. In the measurements, we used a wheel trigger on the car to control the snapshot distance, which is approximately 0.97 m and corresponding to 0.92 $\lambda$, where $\lambda$ is the wavelength at the center frequency of 285 MHz.[1] This snapshot distance is also used in Sec. IV. At each trigger event, one data block of 4 channel snapshots is recorded and averaged into a single snapshot to increase the signal-to-noise ratio (SNR). The channel is assumed to be approximately stationary over 4 consecutive snapshots, an assumption that is verified. Due to practical constraints, all measurements were performed using vertical polarization only. One should be aware of the limitations of the parameter estimates from such a setup [12], and we have made every effort to validate the directional estimates using 3-dimensional maps and photos of the environments.

By using the SAGE algorithm [13], MPCs with delay, AOA, AOD and complex amplitude were estimated from the measured transfer function matrices. From the analysis in [7], it can be seen that there are line-of-sight (LOS) conditions for most parts of routes 1 and 2, but occasionally with small obstacles blocking the LOS. Routes 3 and 4, on the other hand, are completely non line-of-sight (NLOS). In the following investigations, routes 1 and 2 are processed together and named group 1. This group is mostly LOS and partially obstructed LOS. Similarly, routes 3 and 4 are named group 2 and this group is completely NLOS.

## III. Clustering and Tracking Method

Since the COST 2100 channel model is based on the concept of clusters, a joint clustering and tracking algorithm [14] is used to identify clusters and determine their time-variant properties from the measurements. The KpowerMeans clustering algorithm [15] is implemented to cluster each temporal snapshot of the channel, while a Kalman filter [16] is designed to track clusters from snapshot to snapshot. Previous research [17] has shown that the cluster time-variant behavior can be obtained with this joint algorithm.

MPCs extracted by the SAGE algorithm are used as the input to this joint clustering and tracking algorithm. In the first step, the KpowerMeans clustering algorithm performs clustering based on the values of the delay, AOD, AOA and power of each MPC from one measured snapshot. Each cluster is characterized by its centroid position, which is determined by cluster delay, cluster power, cluster AOD, and cluster AOA, as well as by its intra-cluster spreads, including cluster delay spread, cluster AOD spread, and cluster AOA spread. The identified clusters for a particular snapshot are known as current clusters. In the next step, a Kalman filter is applied to track the clusters over different snapshots. Based on the current clusters and clusters from the previous snapshot, the Kalman filter provides a prediction of the cluster centroids for the next snapshot and its state is also updated. If possible, the current clusters are associated with those from the previous snapshot and are then regarded as tracked clusters. Otherwise, untracked clusters in the previous snapshot are regarded as dead, and untracked clusters in the current snapshot are considered as

[1] Snapshots with distance 0.115 $\lambda$ were actually measured, but every 8th snapshot is used for further parameterization analysis.

new-born clusters. In this way, we could obtain the time-variant properties of clusters.

The number of MPCs extracted with the SAGE algorithm is 200 for each snapshot; MPCs with a power 30 dB lower than the peak power are discarded from further analysis. To ensure tracking stability, a sliding window with a length of 2 snapshots is chosen [14]. A 1% cluster power threshold is set to ensure that the identified clusters do not carry less than 1% of the total received power. In addition, if the power of a tracked cluster never exceeds 2.5% of the total received power somewhere during its lifetime, this tracked cluster is not taken into account in the subsequent analysis. By considering the map of the environments and in order to avoid cluster splitting, the maximum number of clusters is chosen as 12, which is well above the extracted average number of clusters, see the results in Sec. IV-B.

## IV. Channel Model Parameters

In this section, the methodologies for the parameterization are studied in detail. Our goal is to extract the required parameters for the COST 2100 channel model based on the 300 MHz outdoor measurements. All the extracted parameters are listed in Table I.

### A. Cluster Visibility Region and Transition Region

Cluster visibility regions are typically assigned to clusters in such a way that when an Rx is inside a visibility region (VR), the cluster assigned to this visibility region is active (contributes to the impulse response). The size of a cluster visibility region is thus linked to the lifetime of a cluster: assuming a stationary environment, the lifetime of a cluster is determined by the number of snapshots over which the cluster is sequentially active. The product of the cluster lifetime and the snapshot distance is called cluster life distance.

There is a general difficulty in extracting the size of cluster visibility regions from a single measured route. For the measured route, the Rx does not always go through the center of the cluster visibility regions. We propose a method for finding the relation between the cluster visibility region radius and the measured cluster life distance as follows. Assume that the cluster visibility region is a circle, and the radius of the circular visibility region $R$ is deterministic. Further assume that the measured route traverses the circular visibility regions at a random (uniformly distributed) distance $D$ from the respective centers of the cluster visibility regions. Given this geometry, the length of an intersection between a measured route and a cluster visibility region is

$$L = \begin{cases} 2\sqrt{R^2 - D^2} & 0 \le D \le R, \\ 0 & \text{otherwise.} \end{cases} \tag{1}$$

Now, the average cluster life distance is

$$\Gamma \triangleq E[L] = \int_0^R 2\sqrt{R^2 - x^2}\, f_D(x)\, \mathrm{d}x, \tag{2}$$

where $E[\cdot]$ denotes statistical expectation and $f_D(x)$ is the probability density function for $D$. By solving the integral in (2) for a uniformly distributed $D$, $0 \le D < R$, we obtain

$$\Gamma = \frac{\pi}{2} R, \tag{3}$$

where the factor $\frac{\pi}{2}$ is defined as compensation factor between the cluster visibility region radius $R$ and the average cluster life distance $\Gamma$.

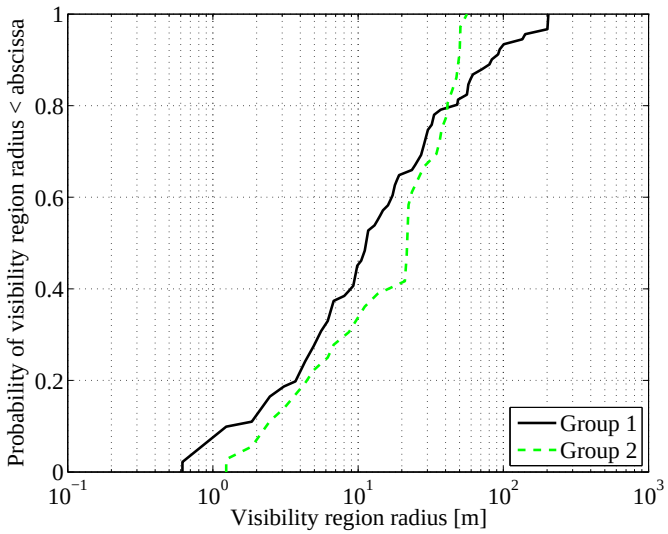


Fig. 2. Distributions of the extracted cluster visibility region radii for the two groups.

We group the measurements into two categories. The measured scenario of group 1, with routes 1 and 2, is categorized as a semi-rural environment where some scatterers have contributed to the impulse response for a long time, which leads to longer cluster life distances, and thus larger cluster visibility region radii. The measured scenario of group 2, with routes 3 and 4, on the other hand, is categorized as a sub-urban area. Scatterers can be blocked more often in this group, and thus smaller cluster visibility region radii are observed. Fig. 2 shows the distributions of the cluster visibility region radii for the two groups. Most of the visibility region radii are in the range of 10 to 100 m (approximately 10 to 100 $\lambda$). The average cluster visibility region radii for groups 1 and 2 are 32.8 and 24.5 m, respectively.

The cluster visibility region is modeled as a circle, where the cluster is active, with radius $R$. Centered in this circle is an effective area, a circle with radius $r$, where the cluster power exceeds a level of 6 dB below its maximum [18]. There is a smooth transition, from the border of the effective area to the border of the active area, taking place in the so-called cluster transition region. The size of the transition region is determined as $T = R - r$, and the extracted sizes of the transition regions are 16.8 m and 12.2 m for groups 1 and 2, respectively.[2]

### B. Number of Clusters and Average MPCs per Cluster

There are two kinds of clusters in the channel model: local clusters and far clusters. Usually a local cluster occurs around

[2] $r$ is extracted in a similar way to $R$.

the Rx. In our measurements, there is one active cluster which is visible along most of the snapshots for the two groups. At the same time, we notice that the distance between this cluster centroid and the Tx is larger than the distance from the cluster centroid to the Rx. In addition, often there is a larger cluster angular spread at the Rx side, compared to the Tx side. These observations indicate that we observe an Rx local cluster in the two measured groups. Far clusters are defined as any clusters that are not local clusters. On average, approximately 6 far clusters ($N_{\mathrm{c}}$) are active for both groups 1 and 2.

Each cluster contains a few MPCs, and the average number of MPCs per cluster ($N_{\mathrm{MPC}}$) is extracted as the ratio between the total number of MPCs and the number of clusters in each snapshot. There are approximately 27 and 48 MPCs per cluster for groups 1 and 2, respectively. For group 2, there are generally more scatterers in the environment, which leads to a larger number of MPCs per cluster, compared to group 1. Here, it should be noted that specular components and dense multipath components [19] are not separated, and all MPCs are considered as specular components.

### C. Single-bounce and Multiple-bounce Clusters

Besides local clusters and far clusters, single-bounce and multiple-bounce clusters are also distinguished in the channel model. Here, we suggest classifying the clusters using their geometric properties. First, we take a look at the AOA and AOD of a cluster and determine whether a ray from the Tx in the cluster AOD direction and a ray from the Rx in the cluster AOA direction can meet each other. If there is no valid intersecting point between the two rays, a multiple-bounce cluster is observed. With a valid intersecting point, we also analyze the total traveling time of these two rays. The traveling time from the Tx to the cluster centroid is $\tau_{\mathrm{Tx}}$ and from the Rx to the cluster centroid is $\tau_{\mathrm{Rx}}$. Theoretically, the difference between the total traveling time of the two rays and the cluster delay $\tau_{\mathrm{delay}}$ should be zero for a single-bounce cluster, but with the measured results, a threshold larger than zero has to be used. The threshold here is set as two times the cluster delay spread $\tau_{\mathrm{ds}}$, since we allow one delay spread offset from both the Tx and Rx sides. In other words, if a valid intersecting point between rays from the Tx and the Rx sides is obtained, and $|\tau_{\mathrm{Tx}} + \tau_{\mathrm{Rx}} - \tau_{\mathrm{delay}}| < 2\tau_{\mathrm{ds}}$ is satisfied, a single-bounce cluster is observed, otherwise it is classified as a multiple-bounce cluster. The relation between the number of single-bounce clusters $N_{\mathrm{SB}}$ and the number of multiple-bounce clusters $N_{\mathrm{MB}}$ is characterized by the cluster selection factor $K_{\mathrm{sel}}$,

$$K_{\mathrm{sel}} = \frac{N_{\mathrm{SB}}}{N_{\mathrm{MB}} + N_{\mathrm{SB}}}. \tag{4}$$

The extracted cluster selection factors are 0.1 and 0.2 for groups 1 and 2, respectively. We conjecture that these low $K_{\mathrm{sel}}$ factors are due to the fact that the measured scenario is peer-to-peer, where the Tx and Rx are only around 2 m above ground, and both surrounded by scatterers along most of the measured routes.

The concept of cluster link delay is introduced in conjunction with the multiple-bounce clusters. The cluster link delay $\tau_{\mathrm{link}}$ is calculated as $|\tau_{\mathrm{Tx}} + \tau_{\mathrm{Rx}} - \tau_{\mathrm{delay}}|$. Hence, for a single-bounce cluster, there is no cluster link delay. The cluster link delay is modeled as an exponential distribution, with its mean and minimum value [2]. Since we use $2\tau_{\mathrm{ds}}$ as our threshold when distinguishing single/multiple-bounce clusters, the cluster link delay for multiple-bounce clusters never goes below $2\tau_{\mathrm{ds}}$. The extracted average cluster link delays are 0.9 and 1.1 μs with minimum values of 0.048 and 0.052 μs for groups 1 and 2, respectively.

### D. LOS Parameters

The LOS component is extracted, based on the AOA, and AOD of the MPC with the strongest received power. In theory, the LOS component should have a matched pair of AOA and AOD and also the strongest power. However, due to uncertainties in vehicle positions and estimation errors of MPC parameters, there might be an offset in the measured AOA and AOD. Here, a maximum 10 degrees mismatch for the AOA and AOD is allowed. In other words, when the mismatch between AOA and AOD of the MPC with the strongest power is smaller than 10 degrees, this MPC is determined as a LOS component.

The size of the LOS visibility region is extracted based on the appearance of the LOS component. When the power of the LOS component goes 6 dB below the maximum LOS power during its lifetime, it enters the transition region where it stays until it disappears. The transition region of the LOS component is defined as the duration between the transition starting and ending points. For group 1, the LOS component exists for almost the whole Rx traveling route; 343 m is observed as the averaged LOS visibility region radius ($R_{\mathrm{LOS}}$) and 93 m as the averaged LOS transition region radius ($T_{\mathrm{LOS}}$). There is no LOS component in group 2 so the sizes of LOS visibility and transition regions are set to zero.

The relation between the power of the LOS component and the other MPCs is denoted as LOS power factor [1],

$$K_{\mathrm{LOS}} = \frac{P_{\mathrm{LOS}}}{P_{\mathrm{tot}} - P_{\mathrm{LOS}}}, \tag{5}$$

where $P_{\mathrm{LOS}}$ is the power of the LOS component and $P_{\mathrm{tot}}$ is the total power for MPCs. The observed mean $K_{\mathrm{LOS}}$ factor is -4.7 dB for group 1 with a variance of 2.0 dB. In group 2, $K_{\mathrm{LOS}}$ is zero since it is a NLOS scenario.

### E. Cluster Power Model

The cluster power $P_{i_c}$ of the $i_c$th cluster, is modeled as [1]

$$P_{i_c} = P_0 \max\{\exp(-k_\tau(\tau_{i_c} - \tau_0)), \exp(-k_\tau(\tau_{\mathrm{cutoff}} - \tau_0))\}. \tag{6}$$

Besides the peak cluster power $P_0$ factor, there are four more parameters in this power model. Parameter $k_\tau$ is the power attenuation coefficient given in unit of dB/μs, and is also called cluster power decay factor. $\tau_{i_c}$ is the cluster delay while $\tau_0$ is the delay of the LOS component. They are both in the unit of μs. The last one is the cut-off delay $\tau_{\mathrm{cutoff}}$, with the unit of μs.

The cluster power decay factor is a result of linear regression analysis of the cluster power versus the cluster delay. The

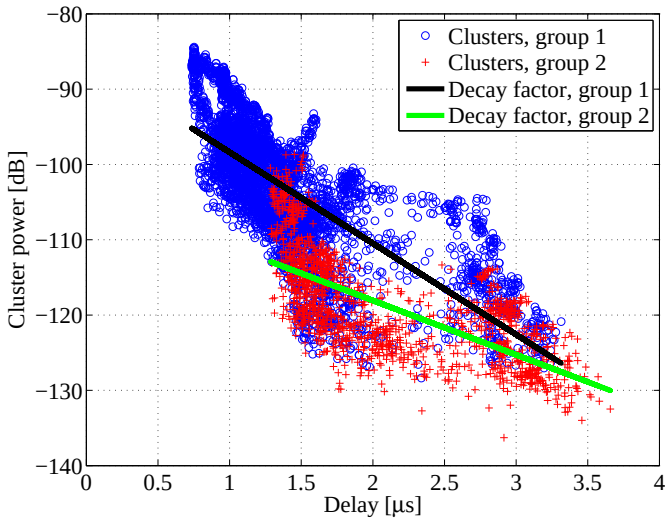


Fig. 3. Cluster power decay factor. Scatter plots show the cluster power vs. the cluster delay. The reference level for the cluster power is the Tx power of 43 dBm. The power decay factors are 12.1 and 7.2 dB/μs for groups 1 and 2, respectively.

slopes in Fig. 3 describe the two power decay factors, which are 12.1 and 7.2 dB/μs for groups 1 and 2, respectively. Moreover, it can be noted that the cluster power has residuals from the regression lines. The residuals are referred as cluster shadowing components, which will be discussed further in Sec. IV-G. The delay of the LOS component is determined by the distance between the Tx and Rx. The cut-off delay is determined as the delay where cluster power has decreased 30 dB from the maximum cluster power. The power of clusters with delays larger than the cut-off delay is modeled as constant, i.e., at a level 30 dB below the maximum cluster power. From the measurements, cut-off delays of 2.4 and 4.2 μs are observed for groups 1 and 2, respectively.

### F. Cluster Spreads

Cluster spreads in delay, AOD and AOA determine the shapes of clusters, and are defined as [1]

$$DS_{\mathrm{c}} = \sqrt{\frac{\sum_i^N P_i(\tau_i - \bar{\tau})^2}{\sum_i^N P_i}}, \tag{7}$$

$$AS_{\mathrm{c}} = \sqrt{\frac{\sum_i^N P_i(\varphi_i - \bar{\varphi})^2}{\sum_i^N P_i}}, \tag{8}$$

where $DS_{\mathrm{c}}$ is the cluster delay spread, $AS_{\mathrm{c}}$ is the cluster angular spread and $N$ is the number of MPCs belonging to each cluster. $P_i$ is the power for the $i$th MPC, $\tau_i$ is the delay and $\varphi_i$ is the AOD/AOA of the $i$th MPC. Furthermore, $\bar{\varphi}$ and $\bar{\tau}$ are power weighted means calculated as

$$\bar{\tau} = \frac{\sum_i^N P_i\tau_i}{\sum_i^N P_i}, \tag{9}$$

$$\bar{\varphi} = \mathrm{angle}(\sum_i^N P_i \exp(j \cdot \varphi_i)), \tag{10}$$

where $j$ is the imaginary unit. The cluster spreads for a particular cluster are computed from the set of MPCs that has been associated with that cluster. The mean value and standard deviation of the extracted cluster spreads are listed in Table I, where $AS_{\mathrm{c}}^{\mathrm{AOD}}$ defines the cluster angular spread at the Tx side and $AS_{\mathrm{c}}^{\mathrm{AOA}}$ is the cluster angular spread at the Rx side. It can be noted that the average cluster delay and angular spreads are smaller in group 1 compared to group 2. The reason is that in group 2, the rich scattering processes around the Tx and Rx increase the spreads of the clusters. The MPCs from scatterers near the Rx in group 2 can, for example, have really large angular spread but are still grouped into one cluster.

### G. Cluster Shadowing

Clusters experience large-scale fading in a similar way to that of MPCs. The cluster shadowing is obtained during the process of estimating the cluster power decay factor, see Sec. IV-E. When the cluster power decay factor is estimated, the linear regression lines provide an expected cluster power for a certain cluster delay. The cluster shadowing is defined as the residual between a cluster power and its expected cluster power [20]. Note, however, that this shadowing is not necessarily related to the physical effects of partial obstructions of clusters by other objects. The observed standard deviations of the cluster shadowing ($\sigma_{Sh_{\mathrm{c}}}$) are 2.05 and 2.27 dB for groups 1 and 2, respectively.

### H. Cross-correlation Coefficients

In order to jointly model cluster spreads and shadowing, the cross-correlation coefficients of different pairs of the cluster spreads and shadowing are considered. We estimate the cross-correlation coefficient between $a$ and $b$ as

$$\rho(a,b) = \frac{\sum_k^M (a(k) - \bar{a})(b(k) - \bar{b})}{\sqrt{\sum_k^M (a(k) - \bar{a})^2 \sum_k^M (b(k) - \bar{b})^2}}, \tag{11}$$

where $\bar{a}$ and $\bar{b}$ are the sample mean of the sets $\{a(k)\}$ and $\{b(k)\}$ with length $M$, respectively, and all the samples are in logarithmic scale [21]. The results for the extracted cross-correlation coefficients are shown in Table I. A high correlation always exists between the delay spread and the angular spreads at both the Tx and Rx sides. Meanwhile, the cluster spreads exhibit low correlation with the cluster shadowing.

## V. Channel Model Validation

The COST 2100 channel model with parameters from Table I is validated by comparing the channel properties of its output with the corresponding measured channel for the outdoor single MIMO link at 300 MHz in this section. Ideally, one should perform validation based on many independent measurements in similar but different environments, but due to the efforts involved in such a task, this is not practically possible. The comparison with the measurements is performed for the following four channel properties: 1) delay spread, 2) spatial correlation, 3) singular value distribution, and 4) antenna correlation.

TABLE I
EXTRACTED PARAMETERS FROM THE 300 MHZ MEASUREMENTS FOR THE COST 2100 CHANNEL MODEL.

| Groups | Group 1 | Group 2 |
|---|---|---|
| Radius of visibility region: | | |
| $\mu_R$[m] | 32.8 | 24.5 |
| Radius of transition region: | | |
| $\mu_T$[m] | 16.8 | 12.2 |
| Number of far clusters: | | |
| $\mu_{N_c}$ | 6 | 6 |
| Number of MPCs per cluster: | | |
| $\mu_{N_{\mathrm{MPC}}}$ | 27 | 48 |
| Cluster selection factor: | | |
| $\mu_{\mathrm{K_{sel}}}$ | 0.1 | 0.2 |
| Cluster power decay factor: | | |
| $\mu_{k_\tau}$[dB/μs] | 12.1 | 7.2 |
| Cluster cut-off delay: | | |
| $\tau_{\mathrm{cutoff}}$[μs] | 2.4 | 4.2 |
| Radius of LOS visibility region: | | |
| $\mu_{R_{\mathrm{LOS}}}$[m] | 343 | 0 |
| Radius of LOS transition region: | | |
| $\mu_{T_{\mathrm{LOS}}}$[m] | 93 | 0 |
| LOS power factor: | | |
| $\mu_{\mathrm{K_{LOS}}}$[dB] | -4.7 | 0 |
| $\sigma_{\mathrm{K_{LOS}}}$[dB] | 2.0 | 0 |
| Cluster angular spreads: | | |
| $\mu_{AS_c^{\mathrm{AOD}}}$[deg] | 14.6 | 18.6 |
| $\sigma_{AS_c^{\mathrm{AOD}}}$[dB] | 2.43 | 2.02 |
| $\mu_{AS_c^{\mathrm{AOA}}}$[deg] | 14.8 | 19.0 |
| $\sigma_{AS_c^{\mathrm{AOA}}}$[dB] | 2.68 | 2.03 |
| Cluster delay spread: | | |
| $\mu_{DS_c}$[μs] | 0.14 | 0.32 |
| $\sigma_{DS_c}$[dB] | 3.66 | 2.05 |
| Cluster link delay: | | |
| $\mu_{\tau_{\mathrm{link}}}$[μs] | 0.85 | 1.02 |
| $\min_{\tau_{\mathrm{link}}}$[μs] | 0.048 | 0.052 |
| Cluster shadowing: | | |
| $\sigma_{Sh_c}$[dB] | 2.05 | 2.27 |
| Cross-correlation coefficients: | | |
| $\rho(DS_c, AS_c^{\mathrm{AOD}})$ | 0.9 | 0.9 |
| $\rho(DS_c, AS_c^{\mathrm{AOA}})$ | 0.9 | 0.9 |
| $\rho(DS_c, Sh_c)$ | 0.0 | -0.1 |
| $\rho(AS_c^{\mathrm{AOD}}, Sh_c)$ | 0.0 | 0.1 |
| $\rho(AS_c^{\mathrm{AOA}}, Sh_c)$ | 0.0 | 0.1 |
| $\rho(AS_c^{\mathrm{AOD}}, AS_c^{\mathrm{AOA}})$ | 0.9 | 0.9 |

$\mu$ denotes expected value, $\sigma$ denotes standard deviation and min denotes minimum value.

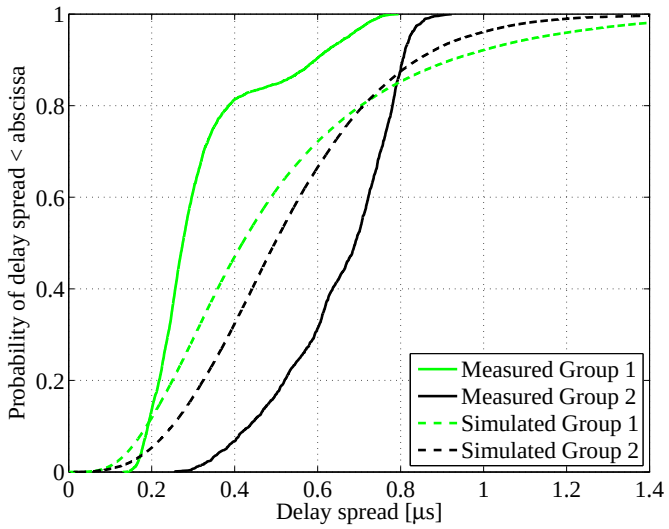


Fig. 4. Delay spreads of the measured and simulated omni-direction antenna responses for groups 1 and 2.

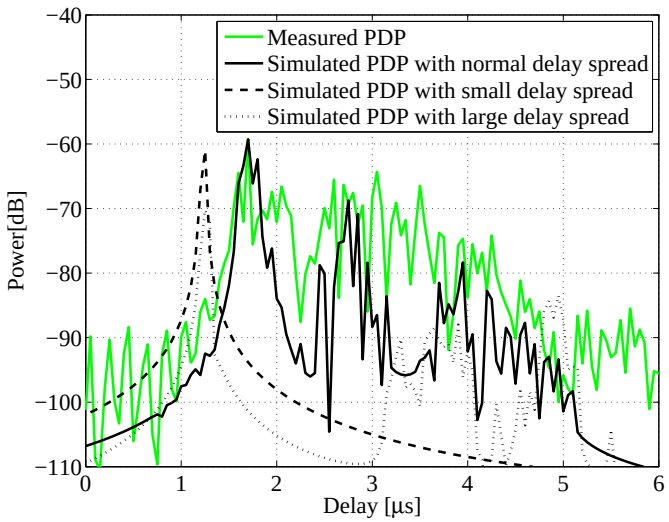


Fig. 5. PDP examples. Measured PDP is extracted from a regular channel under NLOS conditions. Simulated PDPs are for a well represented channel under NLOS conditions and channels with very small and large delay spreads under LOS conditions.

### A. Initial Considerations

The channel model has been implemented in MATLAB by Liu *et al.* [22], and this implementation provides a suitable framework for our validation. The input of this framework is based on both external and stochastic parameters. First, the external parameters include parameters such as frequency, and bandwidth. To be directly comparable with the measured data, the center frequency is set to 285 MHz and the channels are generated for a bandwidth of 20 MHz. The simulated area is defined as a cell with a radius of 500 m. Based on the cluster power decay factors derived in Sec. IV-E, we assume that clusters outside this radius will give a negligible contribution to channel responses. The Tx is placed in the cell center and the Rx is moving according to the measured routes. In order to evaluate the details of delay spreads and spatial correlations, channel snapshots are generated for every 0.115 $\lambda$ movement of the Rx in the simulations. For each simulation run, this sampling distance gives us 5304 simulated snapshots corresponding to the group 1 measurements, and 1570 simulated snapshots corresponding to the group 2 measurements. Besides the external parameters, Table I summarizes all the stochastic parameters that are used as the input of the MATLAB framework. Evaluation, using a group of 100 simulation runs, is carried out for further validation, and for each such simulation run, we have simulated channel snapshots from a route similar to the measured one. This means that the number of channel snapshots used for validation exceeds 50,000 and 15,000 for groups 1 and 2, respectively, which gives us representative statistics. To verify the latter, another independent 100 simulation runs have been performed. By comparing the distributions of delay spreads, spatial correlation, and singular values, similar results were obtained, indicating that a group of 100 simulation runs is enough.

### B. Delay Spread

Delay spread is the normalized second-order central moment of the power delay profile, and defined as [23]

$$S_\tau = \sqrt{\frac{\int_{-\infty}^{\infty} P_\tau \tau^2 d\tau}{\int_{-\infty}^{\infty} P_\tau d\tau} - \mu_\tau^2}, \quad (12)$$

where

$$\mu_\tau = \frac{\int_{-\infty}^{\infty} P_\tau \tau d\tau}{\int_{-\infty}^{\infty} P_\tau d\tau}, \quad (13)$$

$\tau$ is the delay and $P_\tau$ is the corresponding power arriving in the delay interval $[\tau,\ \tau + d\tau]$. The delay spread shows the frequency selectivity of the channel, and it is a fundamental validation metric, affecting other validation metrics such as the singular value distribution. We first compare simulated and measured channels concerning their respective delay spreads. The comparison is performed for channel responses with an omni-directional antenna pattern in azimuth. The delay spreads are computed from the channel power delay profiles (PDPs) by using a noise threshold of 30 dB below the peak power in each PDP. In addition, all PDPs are truncated at 6 μs, and it can be assumed that no significant power will be received after this 6 μs delay.

In Fig. 4, the dashed lines are cumulative distribution functions (CDFs) for the delay spreads from all simulation runs, and the solid lines are CDFs for the delay spreads extracted from the measured raw data. Group 1, which has mostly LOS conditions, shows smaller delay spreads than group 2, which has NLOS conditions. It can be noted that the CDFs for the simulated channels start at smaller delay spreads than the corresponding CDFs for the measured channels. Furthermore, the distributions for the simulated channels have tails with significantly larger delay spreads than those which can be observed from the two measured groups. It can also be noted that in the LOS scenario, the simulated channels result in larger delay spreads, while in the NLOS scenario, the simulated channels show smaller delay spreads for most of the time compared to the measurements. The delay spread differences of the medians between the simulations and measurements are 0.17 and -0.12 μs for groups 1 and 2, respectively. One should note that the measurement area, though we think it is representative for the intended scenarios and that there are differences in the propagation conditions within the area, might not show all possible channel variations when measuring at various places.

To understand the mechanisms behind the observed deviations between the simulated and measured delay spread distributions, we have investigated individual PDPs from simulations and measurements in detail. First, we show an example of a case in which the PDPs of simulated and measured channels agree well, see the two solid curves in Fig. 5. The PDPs indicate channels with rather dense multipath propagation. Next, the two dashed lines in Fig. 5 show examples of PDPs from simulated channels with delay spreads that deviate significantly from what have been observed in the measurements; one of the profiles leads to a very small delay spread, which is smaller than 0.2 μs and the other one causes a very large delay spread, which is larger than 1 μs. The profile leading to the small spread has contributions from only the LOS component and the local cluster, with no far clusters being present. Here, we find a limitation of the COST 2100 channel model when it is applied to outdoor scenarios. In reality, as the measurements indicate, it is not likely to have only one cluster active in an outdoor scenario in a built-up area with a few objects somewhere around Tx and/or Rx, but it can occur in the simulations. In the profile with the large delay spread, a large gap exists between the local cluster and the far clusters. This gap, which causes the delay spread to increase significantly, is observed only in the simulations. In reality, however, the PDP for such a scenario tends to be close to a continuous decay without large gaps. In the channel model, the radius of a cluster is generated according to a log-normal distribution, and thus some small radii exist. As a consequence, the MPCs belonging to the clusters with small radii are squeezed into a small delay region, which causes the gap in the PDP. In conclusion, a truncated log-normal distribution, which takes away the small cluster radii, can provide a better fit for the distribution of delay spreads in an outdoor scenario.

### C. Spatial Correlation

Spatial correlation describes how the channel varies for a certain distance separation, and the normalized spatial correlation is evaluated for the channel envelope as [23]

$$\rho(\Delta d) = \frac{1}{N_d N_f} \sum_d \sum_f \frac{C(|H(d,f)|, |H(d+\Delta d, f)|)}{\sqrt{C(|H(d,f)|)C(|H(d+\Delta d,f)|)}}, \quad (14)$$

where $f$ is the frequency, $d$ is the distance of a certain snapshot, $\Delta d$ is the distance difference between two snapshots, $C$ means the covariance and $|H|$ represents the envelope of the channel, which is achieved from the omni-directional antenna element responses. We choose the envelope correlation since an oscillatory behavior of the averaged complex correlation is observed when the measured route is symmetric relative to the Tx, see routes 1 and 2 in Fig. 1. The symmetric property of the measured route is not representative, but a special case for this particular Tx-Rx arrangement. We investigate the envelope correlation properties for distance differences from 0 to 10 wavelengths. Data subsets with a size of 12 $\lambda$ are used to maintain wide-sense stationarity (WSS) when evaluating the spatial correlation.

In Fig. 6, it can be noted that the match between the simulations and measurements is good for group 2, but not for group 1. The main deviations are in the region of low correlation, hence not so important. When the spatial correlation coefficient is around 0.5, the corresponding spatial distance differences between the simulations and measurements are only 0.2 and 0.1 $\lambda$ for groups 1 and 2, respectively. The simulations have high correlation within a quarter of a wavelength, while the measurements show high correlation within half a wavelength. The spatial correlation is mostly determined by the distribution of the AOA spreads of the MPCs. In general, a large angular spread leads to a low spatial correlation. In measured group 1, the MPCs reach the Rx with a small angular spread since the scatterers are located close to

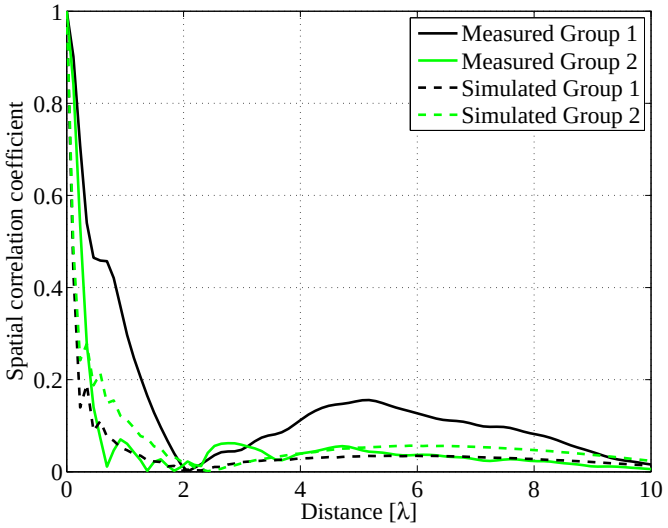


Fig. 6. Spatial correlations of the envelope of the channels both in the measurements and simulations.

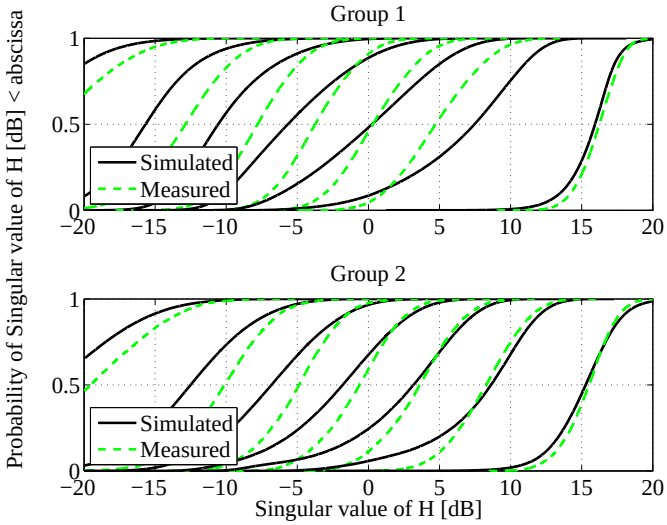


Fig. 7. Distributions of ordered singular values of the measured and simulated channel impulse responses.

TABLE II
COMPARISON OF MEAN AND STANDARD DEVIATION OF THE SINGULAR VALUES BETWEEN THE SIMULATIONS AND MEASUREMENTS.

| Singular values (Ordered) | Group 1 (Sim./Mea.) | | Group 2 (Sim./Mea.) | |
|---|---|---|---|---|
| | Mean [dB] | Std. [dB] | Mean [dB] | Std. [dB] |
| 1 | 15.7/16.2 | 1.8/1.4 | 15.2/15.4 | 2.3/1.8 |
| 2 | 6.7/4.8 | 4.3/2.9 | 7.8/8.2 | 3.9/2.5 |
| 3 | 0.1/0.4 | 4.5/2.8 | 2.5/3.5 | 4.2/2.7 |
| 4 | -5.3/-3.6 | 3.8/2.6 | -2.2/-0.8 | 4.1/2.7 |

the direction of the LOS component; the averaged measured AOA spread is around 39 degrees. As the Rx is moving, the channel is changing slowly. In measured group 2, more scatterers surround the Rx, and an AOA spread of 68 degrees is observed. Compared to group 1, this AOA spread is larger and leads to a lower spatial correlation. In the simulations, on the other hand, the clusters are placed uniformly in the cell; the AOA spread of the simulated MPCs is not controlled, so the two simulated spatial correlations are reduced compared to the values from the measurements. On the other hand, the size of the cluster visibility region also affects the spatial correlation; a longer visibility region radius gives a higher spatial correlation. As described in Sec. IV-A, some clusters have a really large visibility region radii, e.g. the local cluster, though many clusters have a short visibility region radii. An average cluster visibility region radius cannot reflect the real environment well, which in turn leads to the mismatch in the spatial correlation. The variations of the visibility region radius cannot be accurately described solely by an average value and a distribution function is therefore suggested for outdoor environments.

### D. Singular Value Distribution

The capacity at a fixed mean SNR is strongly dependent on the singular value distribution. The singular value is extracted from the normalized channel frequency response by singular value decomposition. For the simulated channels, 7-by-7 channel transfer functions are generated for the two groups, based on the channel model and measured antenna calibration data. All singular values are evaluated at an SNR of 20 dB for both the simulations and measurements.

The channel model shows good agreement with the measurements in terms of the distributions of the singular values obtained from the channel matrices, and thus, in terms of channel capacity, see Fig. 7. The simulated dominant singular value has a mean of 15.7 dB and standard deviation (std.) of 1.8, while the measured one has a mean of 16.1 dB and a std. of 1.4 for group 1. The second largest singular value also matches well with the measured data in group 1. More numeric results are listed in Table II. The fourth singular value is nearly 20 dB lower than the largest singular value in each group, and its contribution to the channel capacity is insignificant. It can thus be noted that the channel model provides a good model of the measured channel regarding channel capacity for outdoor measurements.

### E. Antenna Correlation

Antenna correlation indicates the possible diversity and the richness of the multipath channel in the environment. The correlation coefficient between two antennas is calculated according to

$$\rho_{12} = \frac{E\{H_1 H_2^*\}}{\sqrt{E\{H_1 H_1^*\} E\{H_2 H_2^*\}}}, \tag{15}$$

where $H_1$ and $H_2$ represent the channel response from two antennas, $E\{\cdot\}$ is the expectation operator over all the possible samples of $H_1$ and $H_2$, and $*$ represents the Hermitian transpose. The correlation coefficients for different antenna element offsets are extracted from the measured and simulated channel frequency responses by clockwise and counter-clockwise shifting of antenna elements. A sliding window of length 20 $\lambda$ is used to ensure that we remain in a WSS region when evaluating the antenna correlation. Here, we only

TABLE III
ANTENNA CORRELATIONS FOR ONE SIMULATION RUN OF THE GROUP 1 CHANNELS.

| | | | | | | |
|---|---|---|---|---|---|---|
| Tx side (Measured/Simulated) | | | | | | |
| 1/1 | 0.3/0.3 | 0.2/0.2 | 0.0/0.3 | 0.0/0.3 | 0.1/0.1 | 0.5/0.4 |
| 0.3/0.3 | 1/1 | 0.4/0.1 | 0.1/0.3 | 0.0/0.2 | 0.1/0.2 | 0.2/0.2 |
| 0.2/0.2 | 0.4/0.1 | 1/1 | 0.3/0.2 | 0.1/0.1 | 0.1/0.0 | 0.1/0.2 |
| 0.0/0.3 | 0.1/0.3 | 0.3/0.2 | 1/1 | 0.3/0.0 | 0.2/0.2 | 0.1/0.2 |
| 0.0/0.3 | 0.0/0.2 | 0.1/0.1 | 0.3/0.0 | 1/1 | 0.5/0.4 | 0.4/0.3 |
| 0.1/0.1 | 0.1/0.2 | 0.1/0.0 | 0.2/0.2 | 0.5/0.4 | 1/1 | 0.5/0.3 |
| 0.5/0.4 | 0.2/0.2 | 0.1/0.2 | 0.1/0.2 | 0.4/0.3 | 0.5/0.3 | 1/1 |
| Rx side (Measured/Simulated) | | | | | | |
| 1/1 | 0.3/0.2 | 0.3/0.1 | 0.1/0.2 | 0.2/0.1 | 0.3/0.1 | 0.6/0.1 |
| 0.3/0.2 | 1/1 | 0.2/0.1 | 0.3/0.2 | 0.1/0.1 | 0.3/0.2 | 0.3/0.1 |
| 0.3/0.1 | 0.2/0.3 | 1/1 | 0.1/0.2 | 0.1/0.1 | 0.4/0.1 | 0.3/0.1 |
| 0.1/0.2 | 0.3/0.2 | 0.1/0.2 | 1/1 | 0.7/0.1 | 0.3/0.2 | 0.2/0.1 |
| 0.2/0.1 | 0.1/0.1 | 0.1/0.1 | 0.7/0.1 | 1/1 | 0.4/0.2 | 0.1/0.1 |
| 0.3/0.1 | 0.3/0.2 | 0.4/0.1 | 0.3/0.2 | 0.4/0.2 | 1/1 | 0.1/0.1 |
| 0.6/0.1 | 0.3/0.1 | 0.3/0.1 | 0.2/0.1 | 0.1/0.1 | 0.1/0.1 | 1/1 |

show the 7-element UCDA antenna correlation coefficients by using one simulation run over the area. Otherwise, over many simulation runs, the antenna correlation will finally become low due to the uniform cluster distribution in the channel model.

Table III summarizes the averaged absolute values of the complex correlation coefficients over different WSS regions for one simulation run of group 1 channels at both the Tx and Rx sides. The root-mean-square-errors (RMSE) between the measured and simulated antenna correlation are 0.1 and 0.2 for the Tx and Rx side, respectively. It can be noted that at the Tx side, better agreement between the simulations and measurements is achieved compared to the case at the Rx side. In the measurements, group 1 has a LOS component and the AOA spread of the MPCs is only 39 degrees, which leads to the high antenna correlation at the Rx side. In the simulations, however, the clusters are placed uniformly in the cell which causes the large angular spread at the Rx side, and leads to the lower Rx antenna correlation. Similarly, the RMSE of antenna correlation at the Tx side is 0.3 while 0.1 at the Rx side for one simulation run of the group 2 channels, which means larger differences are observed at the Tx side. The measured angular spread at the Tx side is small, and most of the MPCs stem from the trees and buildings in the upper north direction, see Fig. 1, thus a high antenna correlation is observed from the measurements. However, in the simulations, the uniformly distributed clusters decrease the antenna correlation, which leads to the large RMSE at the Tx side. In general, when the measured AOD or AOA are close to being uniformly distributed, a good match is achieved with respect to the antenna correlation, but when the angular spread is limited by the environment (the close buildings in our case) the antenna correlation can be underestimated in the simulations.

## VI. CONCLUSION

The COST 2100 channel model framework is a good platform for realistic MIMO simulations. Parameterization and validation of the channel model for the scenarios of interest are necessary to get realistic and representative results. In this paper, we parameterize and validate the channel model for outdoor environments based on channel measurements at 300 MHz. Table I summarizes the stochastic parameters of the outdoor MIMO measurements at 300 MHz. These parameters provide a basis for the usage of the channel model in outdoor environments. By applying the extracted parameters to the COST 2100 MATLAB channel model, we perform validation by four means: delay spread, spatial correlation, singular value distribution and antenna correlation. The spatial correlation shows high similarity within a quarter of a wavelength between the simulations and measurements. Similarly, the singular value distributions for the three dominant eigenvalues also show good agreement. Regarding the delay spreads, some mismatch occurs for the two investigated groups, one has 0.17 μs difference and the other has -0.12 μs difference for the delay spread of the medians. Antenna correlation shows good agreement between the simulations and measurements, when there are uniformly distributed scatterers around the antennas. Otherwise, there might be some mismatch. In addition, the validation processes also provide a deep insight of the channel model behavior for outdoor environments.

TABLE IV
SUGGESTED MODIFICATIONS OF THE COST 2100 CHANNEL MODEL FOR A 300 MHZ OUTDOOR SCENARIO.

| Parameters | In the model | Suggested modifications |
|---|---|---|
| Cluster delay spread | log-normal | truncated log-normal |
| Cluster visibility region | mean | mean and variance |

In general, the COST 2100 channel model works well for representing the 300 MHz outdoor scenario, however, not all the properties show good agreement. We suggest that with the modifications of the distribution of cluster delay spreads, and cluster visibility regions in the channel model, see Table IV, better results can be obtained. The channel model also enables multi-link MIMO modeling, and studies related to multi-link will be carried out in the future.

## VII. ACKNOWLEDGMENTS

We thank Prof. Andreas F. Molisch for his helpful discussions and suggestions. The authors would also like to acknowledge Dr. Shurjeel Wyne for the clustering implementation and Dr. Ruiyuan Tian for discussions of the cluster tracking algorithm.

## REFERENCES

[1] L. M. Correia, "The COST 273 MIMO channel model," in *Mobile broadband multimedia networks*, 1st ed., Jordan Hill, Oxford, U.K.: Academic Press, 2006, pp. 364-384.

[2] R. Verdone and A. Zanella, "Radio channel modeling for 4G networks," in *Pervasive mobile and ambient wireless communications: COST Action 2100 (signals and communication technology)*, 1st ed., London: Springer, 2012, pp. 67-148.

[3] J. Poutanen, F. Tufvesson, K. Haneda, V. Kolmonen and P. Vainikainen, "Multi-link MIMO channel modeling using geometry-based approach," *IEEE Trans. Antennas Propagat.*, vol. 60, no. 2, pp. 587-596, Feb. 2012.

[4] L. Liu, J. Poutanen, F. Quitin, K. Haneda, F. Tufvesson, P. De Doncker, P. Vainikainen and C. Oestges, "The COST 2100 MIMO channel model," *IEEE Wireless Commun.*, vol. 19, issue 6, pp 92-99, Dec. 2012.

[5] J. Poutanen, K. Haneda, L. Liu, C. Oestges, F. Tufvesson and P. Vainikainen, "Parameterization of the COST 2100 MIMO channel model in indoor scenarios," in *Proc. European Conf. on Antennas and Propagat.*, Rome, Italy, 2011, pp. 3603-3610.

[6] K. Haneda, J. Poutanen, L. Liu, C. Oestges, F. Tufvesson and P. Vainikainen, "Comparison of delay and angular spreads between channel measurements and the COST 2100 channel model," in *Proc. Loughborough Antennas and Propagat. Conf.*, Loughborough, U.K., 2010, pp. 477-480.

[7] G. Eriksson, F. Tufvesson, and A. F. Molisch, "Propagation channel characteristics for peer-to-peer multiple antenna systems at 300 MHz," in *Proc. IEEE Global Commun. Conf.*, San Francisco, USA, 2006, pp. 1-6.

[8] K. Wiklundh and G. Eriksson, "A study of the capacity for different element spacing on compact MIMO platforms," in *Proc. Personal, Indoor and Mobile Radio Commun.*, Cannes, France, 2008, pp. 1-5.

[9] R. S. Thomä, D. Hampicke, A. Richter, G. Sommerkorn and U. Trautwein, "MIMO vector channel sounder measurement for smart antenna system evaluation," *European Transactions on Telecommunications*, vol. 12, no. 5, pp. 427-438, Sep./Oct. 2001.

[10] RUSK channel sounder – Measurement principle. [Online]. Available: http://www.channelsounder.de/ruskchannelsounder.html.

[11] G. Eriksson, S. Linder, K. Wiklundh, P. Holm, P. Johansson, F. Tufvesson and A. Molisch, "Urban peer-to-peer MIMO channel measurements and analysis at 300 MHz," in *Proc. IEEE Military Commun. Conf.*, San Diego, CA, USA, 2008.

[12] M. Landmann, M. Käske and R. S. Thomä, "Impact of incomplete and inaccurate data models on high resolution parameter estimation in multidimensional channel sounding," *IEEE Trans. Antennas Propagat.*, vol. 60, no. 2, pp. 557-573, Feb. 2012.

[13] B. H. Fleury, M. Tschudin, R. Heddergott, D. Dahlhaus and K. Ingeman Pedersen, "Channel parameter estimation in mobile radio environments using the SAGE algorithm," *IEEE J. Select. Areas Commun.,* vol. 17, no. 3, pp. 434-450, Mar. 1999.

[14] N. Czink, R. Tian, S. Wyne, F. Tufvesson, J. P. Nuutinen, J. Ylitalo, E. Bonek and A. F. Molisch, "Tracking time-variant cluster parameters in MIMO channel measurements," in *Proc. China Commun. Conf.*, Shanghai, China, 2007, pp. 1147-1151.

[15] N. Czink, P. Cera, J. Salo, E. Bonek, J. Ylitalo and J. P. Nuutinen, "A framework for automatic clustering of parametric MIMO channel data including path powers," in *Proc. Veh. Technol. Conf.*, Montreal, Canada, 2006, pp. 1-5.

[16] S. M. Kay, "Kalman filters," in *Fundamentals of Statistical Signal Processing, Estimation Theory*, 1st ed., Upper Saddle River, NJ, USA: Prentice Hall, 1993, pp. 419-476.

[17] N. Czink, R. Tian, S. Wyne, G. Eriksson, T. Zemen, J. Ylitalo, F. Tufvesson and A. F. Molisch, "Cluster parameters for time-variant MIMO channel models," in *Proc. European Conf. on Antennas and Propagat.*, Edinburgh, U.K., 2007, pp.1-8.

[18] H. Asplund, A. A. Glazunov, A. F. Molisch, K. I. Pedersen and M. Steinbauer, "The COST 259 directional channel model-part II: macrocells," *IEEE Trans. Wireless Commun.*, vol. 5, no. 12, pp. 3434-3450, Dec. 2006.

[19] J. Poutanen, J. Salmi, K. Haneda, V. Kolmonen and P. Vainikainen, "Angular and shadowing characteristics of dense multipath components in indoor radio channels," *IEEE Trans. Antennas Propagat.*, vol. 59, no. 1, pp. 245-253, Jan. 2011.

[20] S. Wyne, A. F. Molisch, G. Eriksson, P. Almers, J. Karedal and F. Tufvesson, "Outdoor-to-indoor office MIMO measurements and analysis at 5.2 GHz," *IEEE Trans. Veh. Technol.*, vol 57, no. 3, pp. 1374-1386, May 2008.

[21] A. Algans, K. I. Pedersen and P. E. Mogensen, "Experimental analysis of joint statistical properties of azimuth spread, delay spread, and shadow fading," *IEEE J. Select. Areas Commun.*, vol. 20, no. 3, pp. 523-531, Apr. 2002.

[22] L. Liu, N. Czink and C. Oestges, "Implementing the COST273 MIMO channel model," in *Proc. NEWCOM-ACoRN Joint Workshop*, Barcelona, Spain, 2009.

[23] A. F. Molisch, *Wireless Communications*, 2nd ed., Chichester, West Sussex, U.K.: Wiley, 2005.